Journal of Applied Polymer Science

WILEY

Applied Polymer SCIENCE

RESEARCH ARTICLE OPEN ACCESS

Self-Crosslinkable Bacterial Cellulose/Chitosan/Pectin Injectable Hydrogels: Design, Characterization and Preliminary Biological Performance

Nabanita Saha[1,2] | Fahanwi Asabuwa Ngwabebhoh[1,3] | Oyunchimeg Zandraa[1] | Mainak Chaudhuri[1] | Nibedita Saha[4] | Diana Solovyov[5] | Girts Salms[6] | Arita Dubnika[7,8] | Alejandro Sosnik[5] | Tomas Saha[4] | Petr Saha[1,4]

[1]Centre of Polymer Systems, Tomas Bata University in Zlin, Zlin, Czech Republic | [2]Department of Polymer Engineering, Faculty of Technology, Tomas Bata University in Zlin, Zlin, Czech Republic | [3]Department of Chemistry, Kocaeli University, Kocaeli, Turkey | [4]University Institute, Tomas Bata University in Zlin, Zlin, Czech Republic | [5]Laboratory of Pharmaceutical Nanomaterials Science, Faculty of Materials Science and Engineering, Technion—Israel Institute of Technology, Haifa, Israel | [6]Institute of Stomatology, Riga Stradins University, Riga, Latvia | [7]Baltic Biomaterials Centre of Excellence, Headquarters at Riga Technical University, Riga, Latvia | [8]Insitute of Biomaterials and Bioengineering, Faculty of Natural Science and Technology, Riga Technical University, Riga, Latvia

Correspondence: Nabanita Saha (nabanita@utb.cz)

Received: 20 March 2025 | **Revised:** 18 July 2025 | **Accepted:** 22 July 2025

Funding: This work was supported by the Technology Agency of the Czech Republic, M-ERA.NET (TH71020005).

Keywords: antibacterial activity | biomaterials | biomedical applications | biopolymers | biopolymers and renewable polymers | crosslinking | cytotoxicity | injectable hydrogel | swelling | synthesis and processing techniques

ABSTRACT

In this study, multifunctional polysaccharide-based injectable hydrogels were developed using chitosan (CS) and dialdehyde bacterial cellulose (D-BC), interpenetrated with pectin (PT). The hydrogels exhibited rapid gelation, good water retention, and injectability under physiological conditions. Comprehensive characterization was performed to assess their chemical structure, internal morphology, thermal stability, and rheological behavior. The formation of dynamic Schiff base bonds between amine groups of CS and aldehyde groups of D-BC facilitated efficient crosslinking, resulting in rapid gelation and favorable swelling properties. The hydrogels also demonstrated shear-thinning behavior, contributing to their injectable and self-supporting characteristics. In vitro biocompatibility was evaluated over 21 days using gingival mesenchymal stem cells (GMSCs), with all formulations maintaining over 80% cell viability, confirming their cytocompatibility. Antibacterial assays revealed significant inhibition of *Staphylococcus aureus*, indicating promising antimicrobial performance. The 3D hydrogel networks provided a porous and stable structure suitable for cellular infiltration and tissue integration. Overall, this work presents a green, bio-based approach for fabricating injectable hydrogels with tunable physicochemical and biological properties, offering a potential platform for soft tissue repair applications, particularly in maxillofacial regeneration.

1 | Introduction

Tissue repair and regeneration is a multidisciplinary field that focuses on developing materials and strategies by integrating principles and knowledge from chemistry, engineering, biology, and physics [1, 2]. Among its various applications, oral and maxillofacial tissue engineering remains one of the most challenging areas due to the complex physiological structures involved. These include intricate tissue architectures, specialized sensory organs, facial skeletal linings and coverings, and a dense network of nerves and blood vessels [3, 4]. Over the years, various approaches, particularly autografts and allografts, have been explored to treat

and restore maxillofacial tissues [5, 6]. However, these methods present significant limitations, including limited availability in the case of autografts and the risk of immunogenic rejection with allografts [7, 8]. These drawbacks hinder the widespread clinical use of such implants. Consequently, tissue regeneration has emerged as a promising and clinically relevant alternative for repairing and reconstructing tissues in the maxillofacial region.

Injectable hydrogels (IHs) have gained significant attention in biomedical applications due to their three-dimensional (3D) network structure, shear-thinning behavior, and excellent biocompatibility [9, 10]. These materials serve as soft scaffolds for in situ drug delivery and tissue repair, offering minimally invasive administration, high loading capacity, controlled release, and low toxicity [11–13]. Their versatility allows adaptation to various delivery routes, including parenteral and non-parenteral methods [14, 15]. Typically composed of hydrophilic natural and/or synthetic polymers, hydrogels are formed through chemical or physical crosslinking, resulting in a network capable of retaining large amounts of water or biological fluids. This water-absorbing ability is attributed to the presence of polar functional groups such as hydroxyl, carboxyl, amine, and amide groups, which also support favorable interactions with physiological tissues and promote a moist environment conducive to cell proliferation and tissue regeneration [16, 17]. Hydrogels can be categorized based on composition (natural, synthetic, or hybrid), gelation mechanisms, biodegradability, charge (anionic, cationic, or neutral), swelling capacity, and porosity [18–23]. This classification reflects their wide-ranging applicability in biomedicine, including use in contact lenses, wound dressings, hygiene products, drug delivery systems, and tissue engineering scaffolds [24]. Despite their promise, challenges such as high production costs and scalability limit broader clinical translation and commercialization. Therefore, continued development of cost-effective, high-performance hydrogel systems remains essential. Innovations in materials, especially those based on biocompatible, injectable, and self-healing hydrogels, are key to advancing therapies for tissue regeneration and controlled drug delivery [25, 26].

For this reason, hydrogels have gradually become a breaking point research topic for biomaterial scientists, where several natural, synthetic, and hybrid polymer hydrogel systems are extensively synthesized and studied [27]. Emerging research on hydrogels includes FDA-approved formulations, clinical trials, biomedical applications, molecular-level investigations, and advanced crosslinking strategies. The continued development of natural, synthetic, and hybrid hydrogel systems is expanding their therapeutic applications to address a broader range of medical conditions and complications. Given these advancements, as well as the existing limitations and design challenges—particularly in the fabrication of injectable formulations, future research is expected to focus on more efficient and innovative hydrogel-based applications [28, 29]. Among the various options, polysaccharide-based hydrogels have garnered significant interest, especially those utilizing Schiff-base linkages or dynamic imine chemistry as crosslinking mechanisms. These systems are widely studied due to their high sensitivity, excellent flexibility, superior recyclability, self-healing capabilities, stimuli-responsiveness, and strong tissue adhesion [10, 18, 30]. Furthermore, the chemical functionality of polysaccharides, such as carboxyl, hydroxyl, and amino groups, can be readily modified to enhance their properties and facilitate the formation of robust crosslinked networks [31, 32].

This study focused on the development of a fully polysaccharide-based injectable hydrogel system, formulated without the use of toxic crosslinking agents or synthetic monomers. The self-crosslinked hydrogels consist of chitosan (CS) and dialdehyde bacterial cellulose (D-BC), interpenetrated with pectin (PT), to form a CS/PT/D-BC hydrogel network. The crosslinking mechanism, based on dynamic Schiff base bonds between amine groups on chitosan and aldehyde groups on oxidized bacterial cellulose, enabled rapid, in situ gelation under physiological conditions. The impact of hydrogel composition on gel stability, injectability, rheological behavior, and cytocompatibility (via cell viability assays) was systematically evaluated. Additional analyses included gel fraction, swelling ratio, porosity, and internal microstructural features, with variations in CS, D-BC, and PT content used to tailor pore architecture and gel performance. Crucially, this hydrogel system introduces a novel biomaterial strategy by integrating three biocompatible polysaccharides to achieve self-crosslinkable, injectable hydrogels with inherent antibacterial activity, shear-thinning flow behavior, and long-term biocompatibility, all without external crosslinkers. Compared to existing injectable hydrogels, this formulation stands out due to its purely natural polymer base, controlled gelation kinetics, and suitability for minimally invasive applications. The combination of favorable physicochemical and biological properties positions this system as a promising candidate for soft tissue repair and regeneration, particularly in oral and maxillofacial tissue engineering.

2 | Experimental

2.1 | Materials

Bacterial cellulose (BC) was synthesized in-house at the Centre of Polymer Systems, Tomas Bata University in Zlín, Czech Republic, and subsequently modified to its dialdehyde form prior to use. Chitosan (CS; high molecular weight, 310–375 kDa; degree of deacetylation, 75%–85%), pectin (PT; galacturonic acid content ≥74% on a dry basis, derived from citrus peel), absolute ethanol (EtOH), ethylene glycol, acetic acid, sodium hydroxide (NaOH), methyl orange, hydroxylamine hydrochloride ($NH_2OH{\cdot}HCl$), hydrochloric acid (HCl; 37% purity), and sulfuric acid (H_2SO_4; ≥95% purity) were all purchased from Sigma-Aldrich, Czech Republic. Sodium periodate ($NaIO_4$) was obtained from Penta Chemicals Ltd. All chemicals were used as received without further purification, and distilled water (dH_2O) was used in the preparation of all solutions.

2.2 | Methods

2.2.1 | Synthesis of Dialdehyde Bacterial Cellulose

The functionalization of bacterial cellulose (BC) was carried out as previously described, with slight modifications [33, 34]. An aqueous BC suspension was prepared by blending the material using a NutriBullet blender at 30,000 rpm for 1 min. The resulting dispersion was mixed with the appropriate amount of $NaIO_4$ under dark conditions at 40°C for 4 h. In a 200 mL glass beaker, approximately 0.2 g (dry weight) of BC was reacted with 0.096 g/mL of $NaIO_4$, with the pH of the reaction mixture adjusted to approximately 4 using 1 M H_2SO_4. The reaction was terminated by

the addition of ethylene glycol, followed by dialysis against dH_2O for 2 days using a dialysis membrane (MWCO: 14.5 kDa), with frequent water changes until a neutral pH was achieved. The resulting dialdehyde-modified bacterial cellulose, referred to as "D-BC," was subsequently frozen and lyophilized for further us.

2.2.2 | Determination of Aldehyde Content

To calculate the degree of oxidation, the hydroxylamine hydrochloride titration method was explored. 0.025 g of the BC and D-BC were dispersed in 15 mL of 0.25 M NH_2OH HCl solution. The 200 μL of 100 ppm methyl orange was added, and the mixture was placed under gentle shaking at 100 rpm for 2 h. The mixtures were then titrated against 0.1 M NaOH solution while controlling pH until the red-to-yellow endpoint reached pH 4 [35, 36]. The aldehyde content (AC %) was calculated based on the volume of NaOH consumed using the following equation:

$$\mathrm{AC}\,\% = \left(\mathrm{MW} \times M\left(V_{D-BC} - V_{BC}\right)/m\right) \times 100 \quad (1)$$

where, m is the mass (g) of BC used, MW is the molecular weight of the cellulose repeating unit (≈162 g/mol), M is the molarity of NaOH (0.1 M), and $V_{\text{D-BC}} - V_{\text{BC}}$ is the consumed amount of NaOH (L). The determined values for the aldehyde content are the average of 3–5 samples.

2.2.3 | Preparation of CS/PT/D-BC Injectable Hydrogels

Stock solutions of CS, PT, and D-BC were initially prepared by dissolving the polymers in phosphate-buffered saline (PBS) and allowing them to hydrate overnight. CS (2% w/v) was dissolved in 1% v/v acetic acid, and the pH was adjusted to between 5.5 and 7.0 using 0.1 M HCl or NaOH. PT (4% w/v) and D-BC (1% w/v) were prepared by dissolving them in PBS at pH 7.4. Injectable hydrogels (IHs) were formulated by varying the concentrations of the three polysaccharide components (CS, PT, and D-BC). First, CS and PT were thoroughly mixed under constant stirring, followed by the addition of D-BC to form homogeneous blends. The compositional variations of the hydrogels, expressed in %w/w, are listed in Table 1. Photographs of the self-crosslinked polysaccharide-based hydrogels, designated S1–S15, are presented in Figure 1a. In addition, Figure 1b–e visually illustrates the gel stability and injectable performance of the developed hydrogel systems. The CS/PT/D-BC hydrogels were stored in a freeze-dried state for further use and analysis.

TABLE 1 | Compositions of formulated CS/PT/D-BC injectable hydrogels in terms of %w/w.

Samples	CS	PT	D-BC
S1	0.25	1.50	0.50
S2	0.50	1.50	0.50
S3	1.00	1.50	0.50
S4	1.50	1.50	0.50
S5	2.00	1.50	0.50
S6	1.00	0.25	0.50
S7	1.00	0.50	0.50
S8	1.00	1.00	0.50
S9	1.00	1.50	0.50
S10	1.00	2.00	0.50
S11	1.00	1.50	0.25
S12	1.00	1.50	0.50
S13	1.00	1.50	0.75
S14	1.00	1.50	1.00
S15	1.00	1.50	1.50

Note: Sample (S3, S9 and S12) have same composition.

2.3 | Characterization of CS/PT/D-BC Injectable Hydrogels

2.3.1 | Porosity Analysis

The porosity percentages of the CS/PT/D-BC IHs were studied by the liquid displacement method. The hydrogel samples (sample size (V_1): 400–800 mm^3; diameter: 14 mm, height: 3-5 mm) were carefully placed into absolute ethanol for 2 h until saturation was reached. The porosity of the samples was then calculated [37] by the following Equation (1):

$$\text{Porosity}\,(P) = \left(W_2 - W_1\right)/\rho V_1 \quad (1)$$

where, W_1 and W_2 are the weights of the hydrogels before and after immersion, respectively. V_1 is the volume of the hydrogels before immersion, and ρ (00078691 g/mm^3 at 37°C) is the constant of the density of ethanol.

2.3.2 | Swelling Study

The swelling analysis was performed with a physiological phosphate buffer solution (pH 7.4) at 37°C. The hydrogels (sample size (V_1): 400–800 mm^3; diameter: 14 mm, height: 3 to 5 mm) were soaked for specific time intervals (5, 10, 15, 20, 25, 30, and 35 min) until equilibrium swelling was reached. The water retention capacities of the hydrogels were then measured [38] by the degree of swelling, which is defined by the following equation (2):

$$\text{Degree of Swelling}\,(\%) = \left(\left[W_s - W_d\right]/W_d\right) \times 100 \quad (2)$$

where W_s and W_d are the weights of the swollen and dried hydrogels, respectively. The equilibrium liquid content (ELC), where the liquid is the physiological saline solution, was calculated [39] by using the following Equation (3):

$$\text{ELC}\,(\%) = \left(\left[M_s - M_0\right]/M_s\right) \times 100 \quad (3)$$

where M_s and M_0 are the weights of swollen hydrogel at equilibrium and the initial dry gel, respectively. At the end of the swelling experiment, the thickness of the swollen gel discs was measured and recorded. The samples were dried in a vacuum oven until constant weights were attained and then reweighed. The gel fraction was calculated [39, 40] by using the following Equation (4):

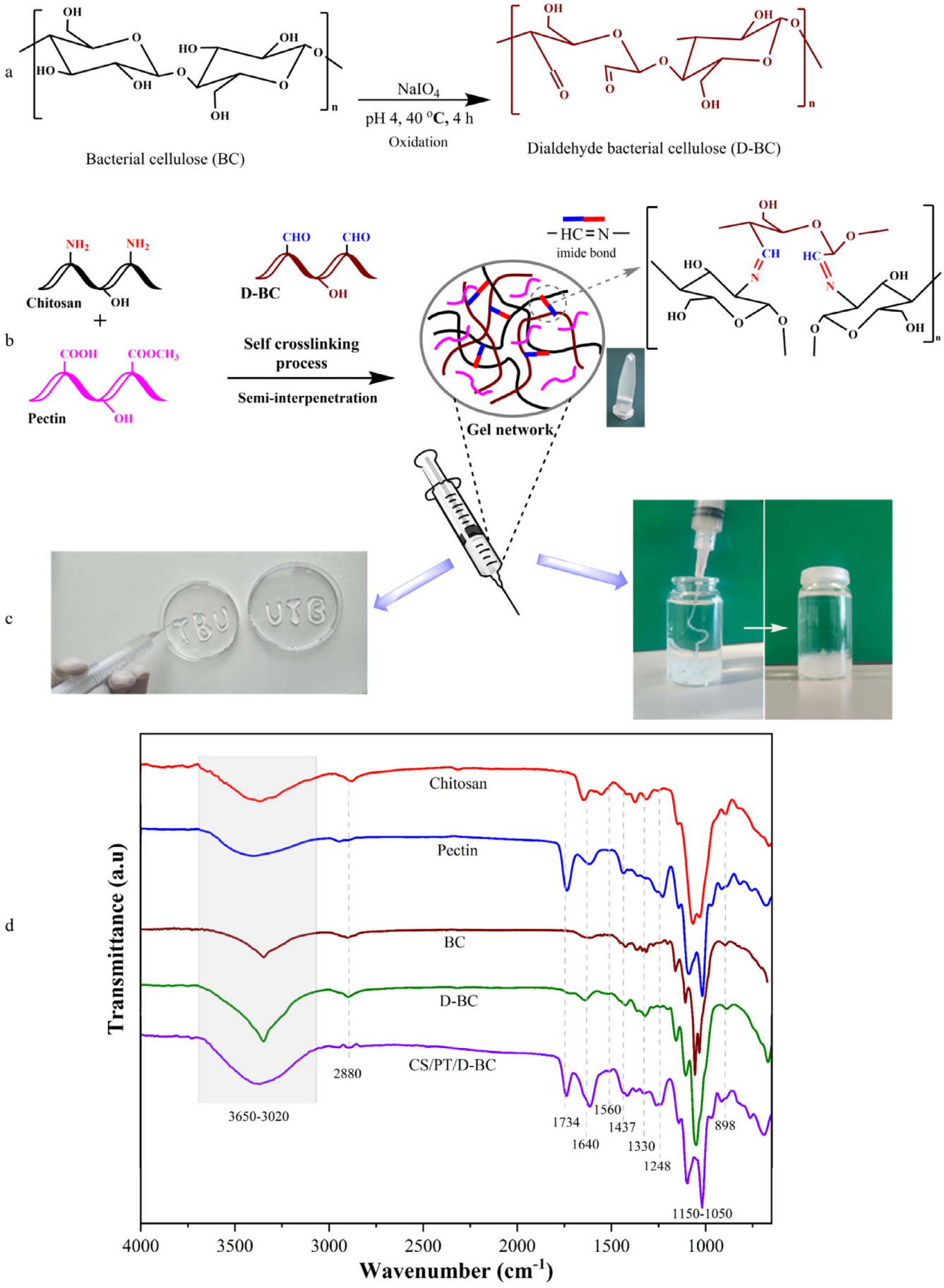

FIGURE 1 | Legend on next page.

FIGURE 1 | Schematic illustration of: (a) BC oxidation process, (b) Crosslinked network formation in the CS/PT/D-BC injectable hydrogel, (c) Hydrogel stability demonstration: (i) post-injection structural integrity on a solid surface and (ii) stability in physiological solution, (d) FTIR spectra comparison of pristine polymers (CS, PT, BC), modified D-BC, and the final CS/PT/D-BC hydrogel. [Color figure can be viewed at wileyonlinelibrary.com]

$$\text{Gel fraction}\,(\%) = \left(M_d / M_0\right) \times 100 \quad (4)$$

where M_d and M_0 are the weights after drying and weights before swelling of the hydrogels, respectively.

2.3.3 | Structural Analysis of CS/PT/D-BC IHs

Fourier transform infrared (FTIR) spectra of the hydrogel samples were recorded using a Nicolet iS5 (Thermo Scientific, USA), scanned at a resolution of 4.0 $cm–1^{-1}$ in the range of 4000 to 400 cm^{-1}. The prepared hydrogels were analyzed for their morphological structures by scanning electron microscope (SEM, FEI, Brno, Czech Republic) at an accelerating voltage of 5 kV. Before analysis, the hydrogels were frozen and freeze-dried, followed by gold coating using a JEOL JFC 1300 Auto Fine Coater (Tokyo, Japan) to enhance surface conductivity.

The thermogravimetric analysis (TGA) of all CS/PT/D-BC injectable hydrogels was conducted using the TA Q500 apparatus (TA Instruments, USA) with approximately 10 mg of each sample placed on a platinum pan, followed by a heating rate of 10°C/min from 25°C to 700°C under nitrogen gas at a flow rate of 40–60 mL/min.

2.3.4 | Rheological Analysis

Rheological measurements were carried out using a rotational rheometer (Anton Paar MCR 502) equipped with a 25 mm parallel plate geometry at a constant temperature of 37°C. To identify the linear viscoelastic (LVE) region, a strain sweep test was first performed over a strain range of 0.1%–100% at a fixed frequency of 1 Hz. Time sweep tests were then conducted over a duration of 0–800 s at a constant frequency of 1 Hz and a strain amplitude of 0.5%. Subsequently, a frequency sweep test was performed by varying the angular frequency from 0.1 to 100 rad/s while maintaining a constant strain of 1%. The storage modulus (G'), loss modulus (G''), and complex viscosity (η^*) were recorded for all hydrogel samples (S1–S15).

2.3.5 | Antibacterial Activity

The antibacterial activity of the CS/PT/D-BC injectable hydrogel samples was evaluated using the agar disk-diffusion method against two bacterial strains: *Staphylococcus aureus* and *Escherichia coli*. Bacterial suspensions were prepared separately from 24-h-old culture colonies of each strain. The bacteria were uniformly spread on sterile Petri dishes containing 25 mL of solidified LB-agar medium (LB supplemented with 1.5% bacteriological agar, Sigma-Aldrich, St. Louis, Missouri, USA). Prior to testing, dried CS/PT/D-BC IH samples (S1–S5), cut into discs of 8 to 10 mm diameter, were sterilized under ultraviolet light for 30 min. The prepared plates were then incubated at 37°C for 24 h. Antibacterial activity was assessed by observing the zones of inhibition formed around the hydrogel samples, indicating the diffusion of antibacterial components. Given that chitosan is known for its intrinsic antibacterial properties, while pectin and dialdehyde bacterial cellulose lack inherent antibacterial activity, only hydrogel formulations containing chitosan (S1–S5) were selected for the antibacterial assay.

2.3.6 | MTS Viability Assay

The cytocompatibility of the injectable hydrogels was evaluated over 21 days using gingival mesenchymal stem cells (GMSCs) via a colorimetric MTS assay (3-(4,5-dimethylthiazol -2-yl)-5-(3-carboxymethoxyphenyl)-2-(4-sulfophenyl)-2H-tetr azolium). Freeze-dried CS/PT/D-BC hydrogels were sterilized under UV light (30 min), equilibrated overnight in Dulbecco's Modified Eagle Medium (DMEM, Sigma-Aldrich), and then cut to fit 96-well plates. GMSCs (1×10^4 cells/well in 100 μL DMEM) were seeded onto the hydrogels and cultured at 37°C under 5% CO_2, with medium changes every 72 h. At days 7, 14, and 21, cell viability was assessed by adding 20 μL of MTS reagent (Promega, Madison, WI, USA) to each well, followed by incubation for 2–4 h. The supernatant was transferred to a fresh 96-well plate, and absorbance was measured at 490 nm (Multiskan GO Microplate Spectrophotometer, Thermo Fisher Scientific). Viability was expressed as a percentage relative to control wells (culture medium only), which were set as 100% viable.

2.4 | Statistical Analysis

Results are displayed as Mean ± Standard error of the Mean. Origin Lab software version 9.0 was used for statistical analysis. The experimental data from all the investigations were analyzed using analysis of variance (ANOVA). A value of $p < 0.05$ was determined as statistically significant.

3 | Results and Discussion

3.1 | Determination of Oxidation Degree and Fabrication of IHs

The average aldehyde (CHO) content in the D-BC was determined to be 57.79% ± 3.16%, confirming successful functionalization. IHs were then prepared by crosslinking CS and D-BC, interpenetrated with PT, primarily through a Schiff-base reaction between the amine groups (-NH_2) of CS and the aldehyde groups of D-BC, forming imine bonds (Figure 1a,b). The resulting network exhibited both covalent and physical crosslinking, contributing to hydrogel stability. Visually, the mixture

gradually increased in viscosity, forming soft, translucent hydrogels (Figure 1c) capable of self-supporting structure at 37°C, making them suitable for cell-based tissue repair and regeneration [9, 16]. The chemical structures of pristine CS, PT, BC, modified D-BC, and the final CS/PT/D-BC hydrogel were characterized and are presented in Figure 11d.

The FTIR spectra of CS exhibited characteristic bands with a broad overlapping peak at 3020 to 3650 cm^{-1} (O–H and $–NH_2$ stretching), a peak at 2880 cm^{-1} (C–H stretching in $–CH_2OH$ and pyranose rings), 1640 cm^{-1} (C=O stretching), and 1437 cm^{-1} (N–H bending) [34]. For PT, the broad band at 3020–3650 cm^{-1} corresponded to O–H stretching, while 2880 cm^{-1} represented C–H vibrations (CH, CH_2, CH_3). Additional peaks appeared at 1734 cm^{-1} (C═O), 1640 cm^{-1} (C-O), 1437 cm^{-1} (CH_3 asymmetric stretching), 1330 cm^{-1}, and 1050 to 1150 cm^{-1} (C-O-C), along with a distinct peak at 898 cm^{-1} (pyranose methylene C–H vibration) [41]. BC showed similar bands at 3020 to 3650 cm^{-1} (–OH), 2880 cm^{-1} (–CH), 1640 cm^{-1} (C═O), 1050 to 1150 cm^{-1} (C–O–C), and 898 cm^{-1} (pyranose methylene) PEVuZE5vdGU [42]. After oxidation, D-BC displayed a new peak at 1734 cm^{-1}, confirming aldehyde (C═O) incorporation [43]. The CS/PT/D-BC hydrogel formation was evidenced by: (1) the disappearance of the CS –NH_2 peak (1580 cm^{-1}) and the D-BC aldehyde peak (1734 cm^{-1}, overlapped by PT's carbonyl stretch). (2) The emergence of a new 1560 cm^{-1} peak, corresponding to the imine (–C═N) stretch from the Schiff-base reaction between CS ($–NH_2$) and D-BC (–CHO) (Figure 1d). This confirms successful crosslinking into a 3D network.

3.2 | Gel Fraction and Porosity of Hydrogels

As shown in Figure 2a, the gel fraction (GF) increased progressively with higher chitosan concentrations across the hydrogel formulations. For instance, samples S1 (0.25% CS), S2 (0.5% CS), and S3 (1.0% CS) displayed GF values of approximately 88.04%, 91.19%, and 92.34%, respectively. The highest GF of 95.37% was observed in sample S5 with 2.0% chitosan, indicating enhanced network crosslinking. This trend aligns with previous findings [44], where increased chitosan content provided more amine groups to react with aldehyde functionalities from D-BC, forming stable imine bonds. Similarly, increasing D-BC content also led to higher gel fraction values. For example, formulations S11–S15, with incrementally increasing D-BC concentrations, showed GF values ranging from 80.68% to 99.77%, supporting prior reports such as Deng et al. [45], where oxidized BC enhanced crosslinking and mechanical integrity. In contrast, increasing pectin content (S6–S10) resulted in a gradual decline in GF, with values dropping from 97.08% to 90.41%. This may be attributed to the increase in mixture viscosity, which hinders effective interaction between reactive groups, as noted in Oh et al. [46].

As shown in Figure 2b, porosity exhibited an inverse relationship with chitosan and D-BC concentrations. Samples with higher CS content (e.g., S5) showed reduced porosity (54.45%), whereas lower-CS samples (e.g., S1) displayed higher porosity (95.68%), consistent with findings by Dang et al. [47]. A similar decreasing trend was observed with increasing D-BC content (S11–S15). However, as pectin concentration increased (S6–S10), porosity also increased, reaching up to 107.12% in S10. This is likely due to the looser network structure caused by pectin's hydrophilic and non-reactive nature, allowing more void formation. These variations are attributed to differences in crosslinking density and network architecture, governed by the balance of covalent (Schiff base) and hydrogen bonding interactions among the polymers. Overall, the data indicate that the hydrogel microstructure and gelation behavior can be finely tuned by adjusting polymer composition, enabling targeted design for specific biomedical applications [48].

3.3 | Swelling Behavior and Environmental Responsiveness

The swelling behavior of the hydrogels prepared with varying concentrations of CS, D-BC, and PT is presented in Figure 3. As observed in Figure 3a, an inverse relationship exists between chitosan concentration and swelling percentage. Sample S1 (0.25% CS) showed the highest swelling capacity, reaching approximately 1720% after 35 min, while S5 (2.0% CS) exhibited the lowest swelling at about 1210%. This decline is attributed to increased crosslinking density and a tighter hydrogel network, reducing pore size and restricting water absorption. These findings are consistent with previous studies on chitosan-based hydrogels [49]. Similarly, increasing pectin content also resulted in decreased swelling behavior. For instance, swelling percentages dropped from 1570% in S6 (0.25% PT) to 1200% in S10 (2.0% PT), indicating that excessive PT may reduce network flexibility due to enhanced viscosity and physical entanglement, which hinders water diffusion [37]. In contrast, increasing D-BC concentration led to a notable improvement in swelling ability. Sample S11 (0.25% D-BC) reached a swelling percentage of 1310%, while S15 (1.5% D-BC) achieved a higher value of 1740%. This enhancement is attributed to the nanofibrillar, porous structure of bacterial cellulose, which facilitates greater water retention and diffusion through the hydrogel network [38, 49]. The swelling behavior of these hydrogels is crucial for biomedical applications, particularly in wound healing and soft tissue engineering, where controlled fluid uptake is required. Furthermore, the hydrogels demonstrated excellent water stability, attributed to the presence of highly crystalline D-BC and robust covalent crosslinking, rendering them insoluble in aqueous environments, an essential feature for in vivo applications. In addition, as shown in Figure 3b, the equilibrium liquid content (ELC) of all samples exceeded 90%, confirming their high water retention capacity. ELC values slightly decreased from 94% to 92% with increasing polymer concentrations, likely due to denser crosslinked networks limiting free water content. This subtle decrease in ELC, alongside the high swelling capacity, reflects the hydrogels' balance between structural integrity and hydrophilic absorption, characteristics that support their potential in tissue repair, especially in environments with varying levels of wound exudate.

The swelling performance of the CS/PT/D-BC injectable hydrogels was evaluated in PBS at physiological pH 7.4 and temperature 37°C to simulate in vivo conditions. As observed, the swelling results demonstrated that the hydrogels possess significant pH and temperature responsiveness, which is critical

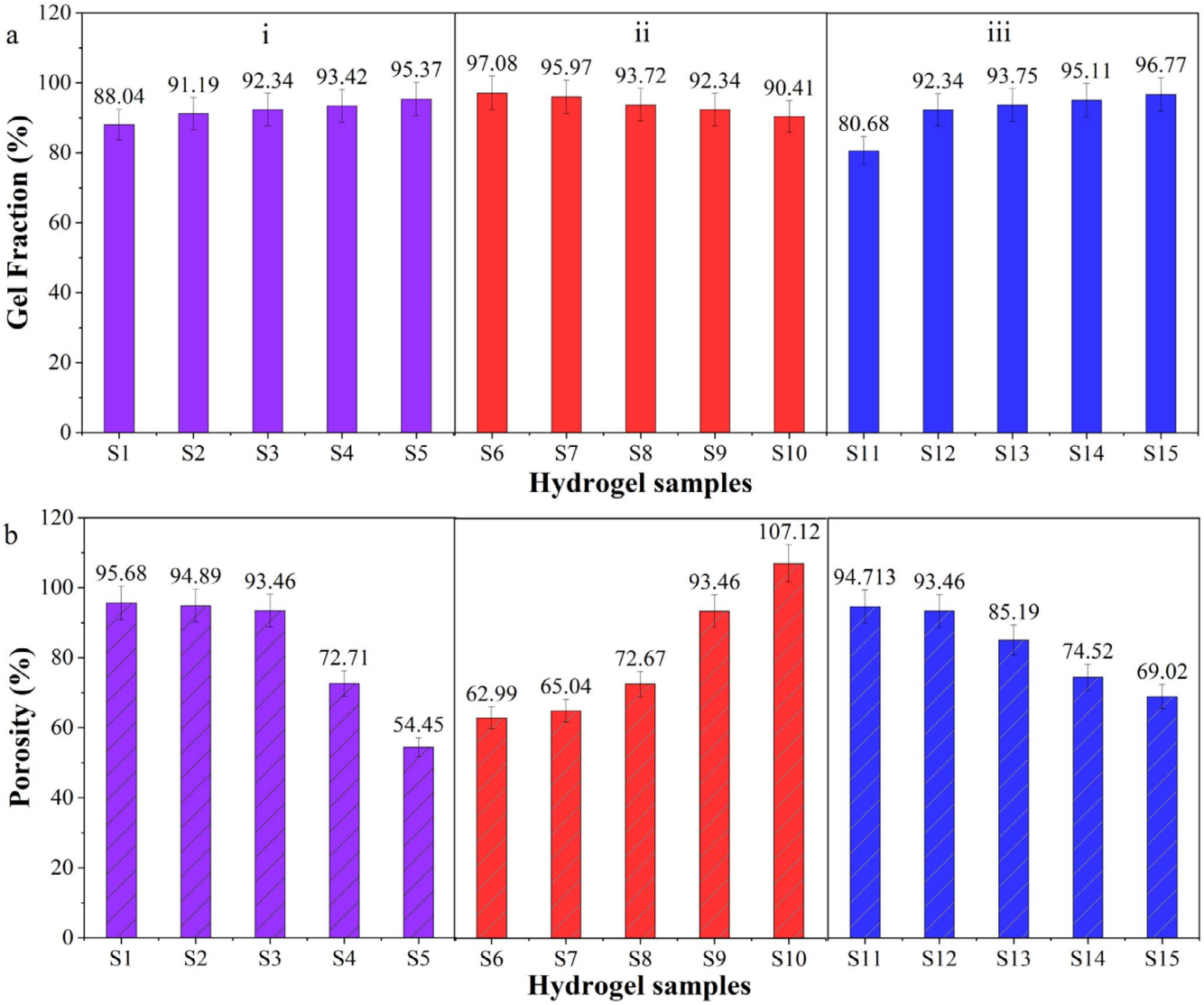

FIGURE 2 | (a) Gel fraction and (b) porosity percentage of CS/PT/D-BC injectable hydrogels with varying polymer ratios: (i) chitosan (S1–S5), (ii) pectin (S6–S10), and (iii) D-BC (S11–S15). [Color figure can be viewed at wileyonlinelibrary.com]

for biomedical applications, particularly in soft tissue environments. At pH 7.4, the hydrogels exhibited stable and reproducible swelling behavior, indicating their structural integrity and compatibility with physiological conditions. The swelling capacity is primarily governed by the ionization of functional groups, namely the amino groups of chitosan and the carboxyl groups of pectin. At neutral pH, partial ionization facilitates electrostatic repulsion and osmotic pressure within the hydrogel matrix, promoting moderate water uptake without compromising gel cohesion [50]. Temperature also plays a vital role in the hydrogel's swelling behavior. At 37°C, an increase in molecular mobility enhances water diffusion into the polymer network [51]. However, the observed equilibrium swelling suggests a thermally stable structure with limited degradation or deformation over time. This temperature responsiveness, coupled with the hydrogels' pH sensitivity, underscores their suitability for in situ gelation and sustained performance in biological environments. In general, these findings confirm that the CS/PT/D-BC hydrogels maintain their functional swelling characteristics under physiological conditions, reinforcing their potential for injectable biomedical applications where stability, responsiveness, and biocompatibility are essential.

3.4 | Surface Morphology Analysis of Hydrogels

The microstructure of freeze-dried CS/PT/D-BC hydrogels was characterized by FE-SEM (Figure 4). The surface morphology revealed an interconnected porous 3D network of nanofibrils, consistent with previous reports by Dayal et al. [52]. Such porous architectures are crucial for facilitating nutrient exchange and metabolite transport [53], yet excessively porous structures may compromise mechanical stability for cell proliferation and tissue regeneration. The hydrogel's physical properties were effectively modulated by varying polymer concentrations. At lower D-BC concentrations (0.25% w/w, samples S11–S15), the hydrogels exhibited highly porous networks. Increasing D-BC content (up to 1.50% w/w) enhanced crosslinking density, resulting in denser fibrous structures with smaller pores and undulated pore walls due to cellulose's

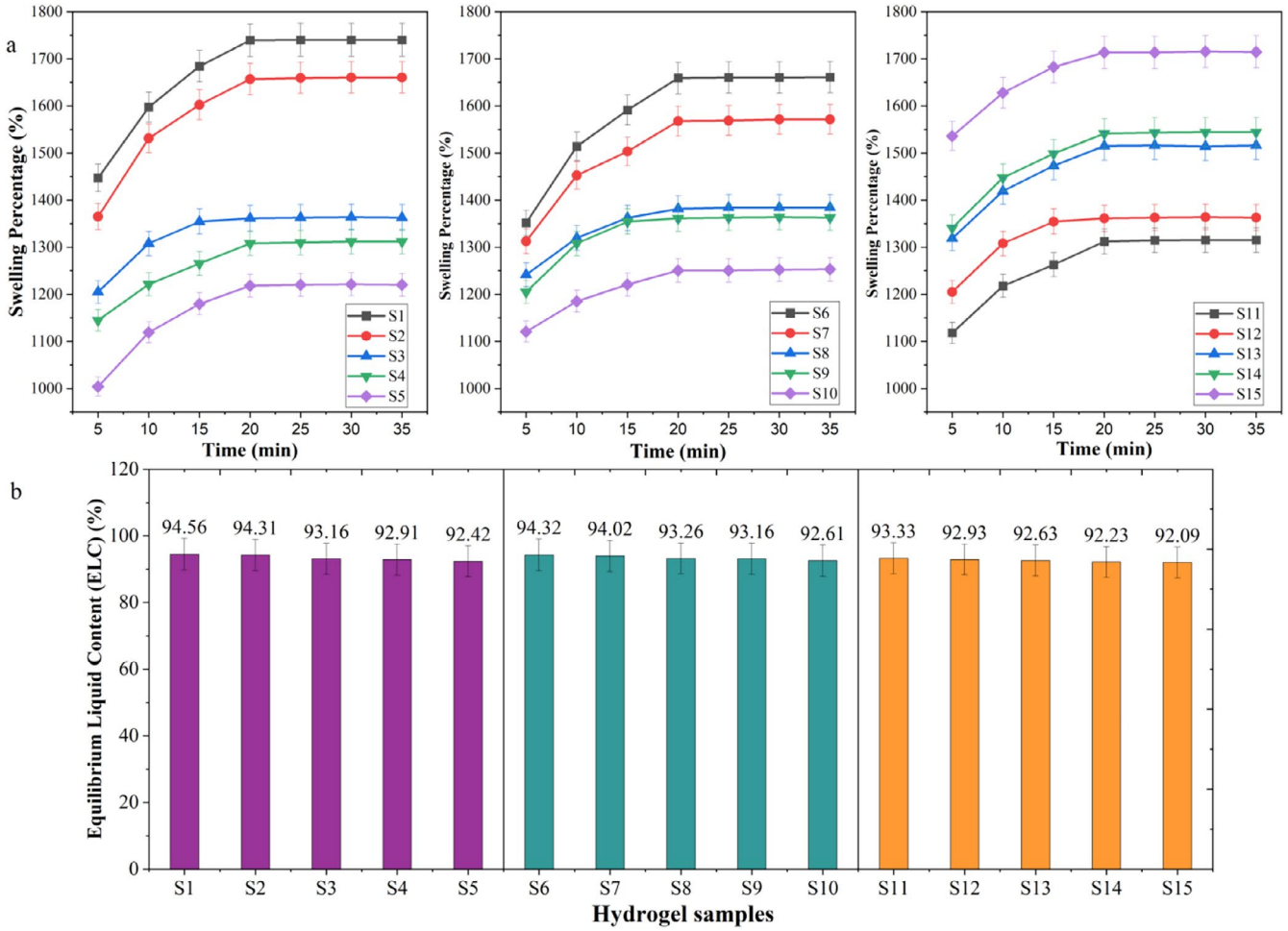

FIGURE 3 | (a) Swelling behavior of CS/PT/D-BC injectable hydrogels with varying polymer ratios: Chitosan (S1–S5), pectin (S6–S10), and D-BC (S11–S15) in PBS (pH 7.4). (b) Equilibrium liquid content of the hydrogels. [Color figure can be viewed at wileyonlinelibrary.com]

reinforcing effect. Similar trends were observed when varying CS and PT concentrations (samples S1–S5 and S6–S10, respectively), where higher polymer content yielded fewer pores and more compact matrices. The enhanced structural stability achieved through chemical crosslinking, combined with the inherent hydrophilicity of the pristine polymers, promotes favorable conditions for cell migration and tissue regeneration [54]. These results demonstrate that the self-crosslinked CS/PT/D-BC hydrogel system offers significant advantages over its individual polymer components for biomedical applications.

3.5 | FTIR Analysis of CS-PT-D-BC IHs

Figure 5a presents the FTIR spectra of CS/PT/D-BC hydrogels (samples S1-S15). The broad absorption band at 3010–3600 cm^{-1} corresponds to overlapping O-H stretching vibrations from CS, PT, and D-BC, along with free $-NH_2$ groups in CS. Characteristic peaks were observed at: 2925 cm^{-1} (C-H stretching in $-CH_2OH$ and pyranose rings), 1620 cm^{-1} (C═O stretching), 1410 cm^{-1} (N-H bending) [34], and 1738 cm^{-1} (C═O stretching in PT and D-BC) [55]. The formation of Schiff-base linkages was confirmed by the appearance of an imine (-C=*N*) stretching vibration at ~1560 cm^{-1} across all samples (S1–S15). The additional peaks at 1265 cm^{-1} (–CH), 1010–1142 cm^{-1} (C–O–C), and 837 cm^{-1} (C–O) were also identified [42]. Notably, the spectra showed minimal variation among samples S1–S15, indicating consistent chemical composition across all formulations. These results demonstrate successful formation of a dynamically crosslinked network through Schiff-base reactions between D-BC's –CHO groups and CS's $-NH_2$ groups, with homogeneous interpenetration of PT throughout the hydrogel matrix.

3.6 | Thermogravimetric Analysis of CS/PT/D-BC IHs

Figure 5b displays the thermogravimetric (TG) analysis of hydrogels with varying CS, PT, and D-BC ratios. All samples exhibited three characteristic degradation stages: (1) 27°C–150°C (bound water evaporation), (2) 150°C–00°C (polymer chain decomposition) [55, 56], and (3) 300°C–575 (char formation). For CS-varied samples (S1–S5), degradation occurred gradually with moderate curve variations, suggesting enhanced crosslinking at higher CS content. PT-varied hydrogels (S6–S10) showed faster decomposition, with second-stage peaks at 270°C (S6) and 227°C (S7–S10). D-BC-containing samples (S11–S15) demonstrated the most rapid degradation (30°C–140°C, 140°C–360°C, and 360°C–550°C for stages 1–3, respectively), indicating reduced

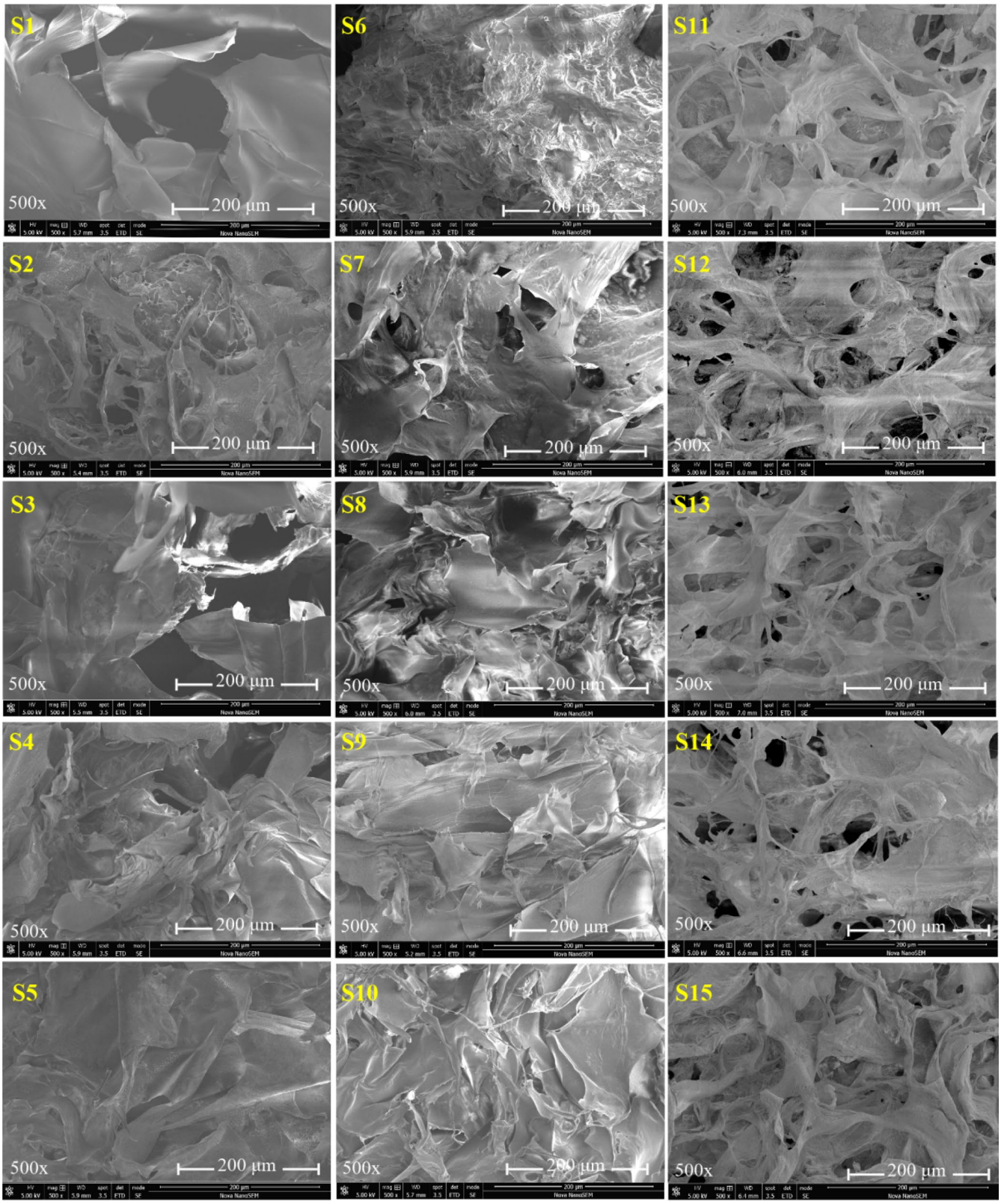

FIGURE 4 | SEM micrographs of freeze-dried hydrogels for varying chitosan ratio (S1–S5), pectin ratio (S6–S10), and D-BC ratio (S11–S15). [Color figure can be viewed at wileyonlinelibrary.com]

thermal stability with increasing D-BC content. This behavior likely stems from D-BC's lower polymer density as the crosslinker [43]. The derivative thermogravimetry (DTG) curves confirmed these three degradation regions for all samples (S1–S15). Greater variation in TG/DTG profiles was observed for CS- and PT-varied hydrogels compared to D-BC-modified ones, reflecting their increased crosslinking density through covalent bonds, hydrogen bonding, and other intermolecular interactions. This

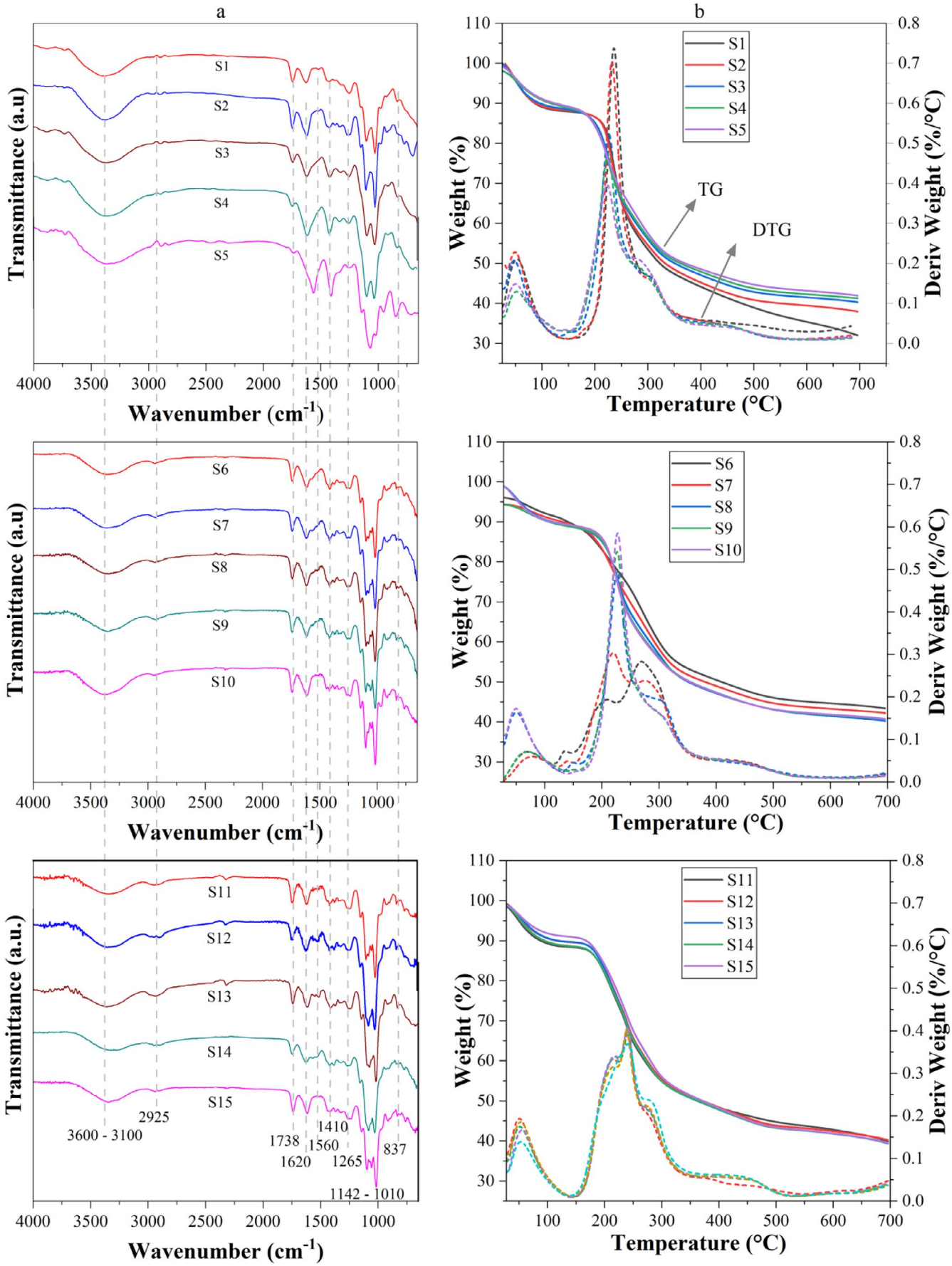

FIGURE 5 | (a) FTIR spectra and (b) TG/DTG curves of CS/PT/D-BC injectable hydrogels with varying polymer concentrations: Chitosan (S1–S5), pectin (S6–S10), and D-BC (S11–S15). [Color figure can be viewed at wileyonlinelibrary.com]

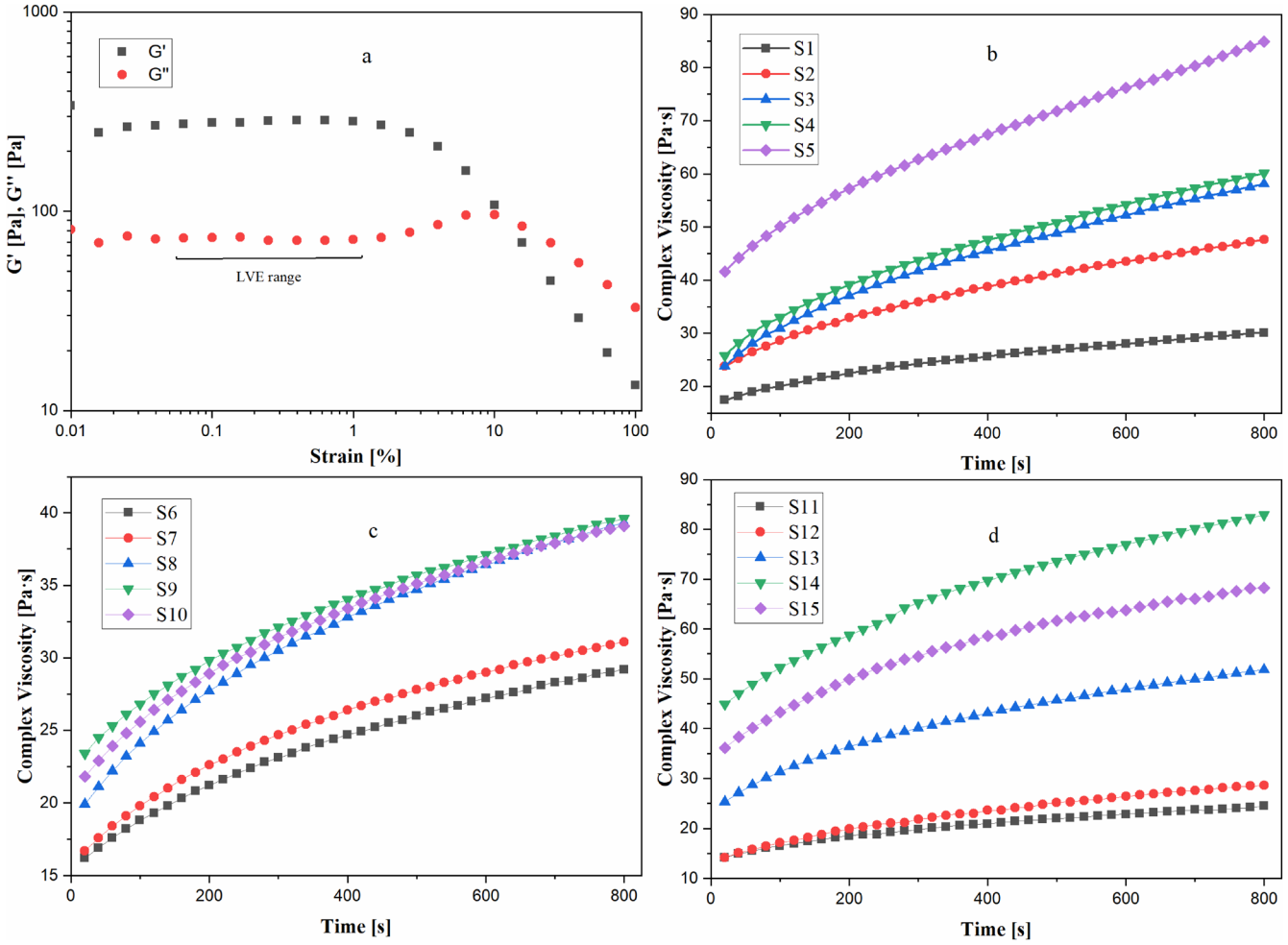

FIGURE 6 | Rheological characterization of injectable hydrogels: (a) Strain sweep showing linear viscoelastic (LVE) range; Complex viscosity profiles for varying concentrations of (b) chitosan (S1–S5), (c) pectin (S6–S10), and (d) D-BC (S11–S15). [Color figure can be viewed at wileyonlinelibrary.com]

created more compact structures in CS/PT-rich formulations. All samples ultimately yielded 25%–28% char residue, consistent with their polysaccharide composition.

3.7 | Rheological Study

The rheological properties of the CS/PT/D-BC injectable hydrogels were quantitatively analyzed to evaluate their practical performance. As shown in Figure 6a, the strain amplitude sweep reveals an intersection between the storage modulus (G') and the loss modulus (G'') at approximately 10% strain, suggesting the gelation point where the hydrogel transitions from a predominantly solid-like to a fluid-like state, approaching the critical gelation threshold [56]. With increasing strain up to 100%, the G' value notably decreases from 100 to 13 Pa, indicating the disruption of the hydrogel network structure. Conversely, when the strain is reduced to 0.01%, both G' and G'' exhibit a linear region between 0.1% and 1% w/w, corresponding to the linear viscoelastic region (LVR) of the hydrogel. The strain sweep results, expressed through the behavior of G' and G'' across varying strain levels, provide insights into the Newtonian response and viscoelastic stability of the material, as illustrated in Figure 6a. The LVR, typically observed at low shear stress, is critical for determining mechanical stability, while the G'/G'' crossover point marks the onset of the gel–sol transition, indicating when the material begins to flow like a fluid [57].

Another key rheological parameter for evaluating injectable hydrogels is complex viscosity, which reflects the material's ability to resist shear deformation at the application site after injection [58]. Figure 6b–d presents the complex viscosity values at 1 Hz for the various hydrogel formulations. The results reveal a substantial increase in complex viscosity over time, indicating that the hydrogels exhibit strong shear-thinning behavior. Variations in complex viscosity across the different samples can be attributed to differences in structural integrity, driven by varying crosslinking concentrations. As shown in Figure 6b–d, hydrogels containing higher amounts of CS and D-BC demonstrated significantly higher complex viscosities compared to those with PT alone. This suggests that complex viscosity is strongly influenced by the concentration of crosslinking polymers, where an increased polymer content leads to enhanced viscosity and structural strength [59]. Moreover, increasing the concentrations of CS, PT, and D-BC in sample sets S1–S5, S6–S10, and S11–S15, respectively, led to a gradual rise in complex viscosity. This trend highlights the positive correlation between polymer content (ranging from 0.25% to 1.5% and 2% w/w) and

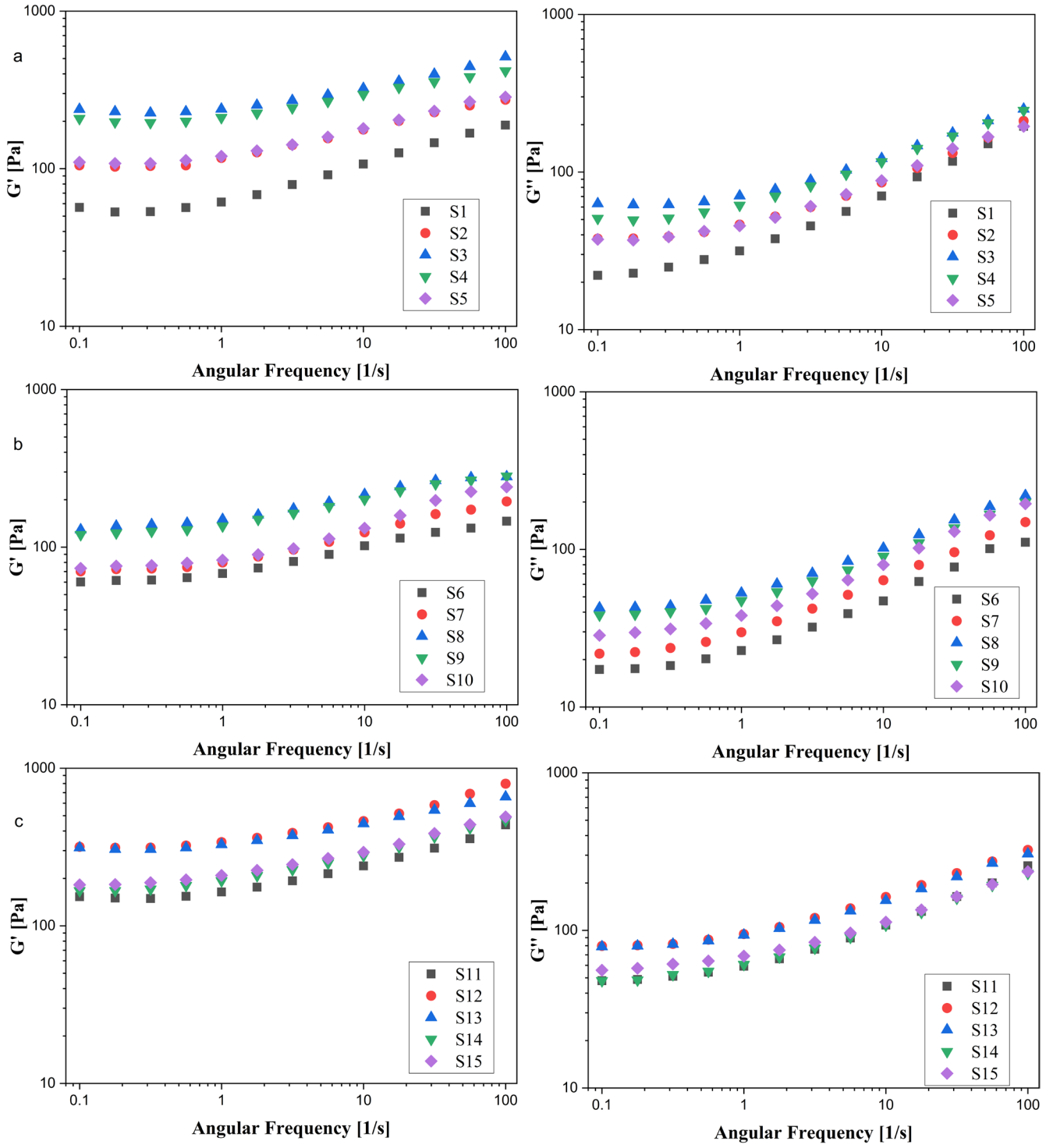

FIGURE 7 | Rheological behavior of injectable hydrogels based on storage (G') and loss modulus (G'') as a function of oscillatory frequency for varying concentrations of (a) chitosan (S1–S5), (b) pectin (S6–S10) and (c) D-BC (S11–S15). [Color figure can be viewed at wileyonlinelibrary.com]

the hydrogels' resistance to shear deformation, thereby improving their mechanical stability and flow behavior. The observed effect in PT-based samples may also be linked to the enhanced stabilization of the gel network.

Frequency sweep experiments were conducted on the CS/PT/D-BC injectable hydrogels to investigate their viscoelastic behavior. As shown in Figure 7, all formulations exhibited elastic-dominant characteristics, with the G' consistently higher than the G'') across the tested frequency range. This was observed for samples S1–S5 (varying CS content), S6–S10 (varying PT content), and S11–S15 (varying D-BC content). The maximum G' values ranged from 56 to 238 Pa for S1–S5, 60–129 Pa for S6–S10, and 153–317 Pa for S11–S15. In comparison, the G'' values were 22–63 Pa, 17–42 Pa, and 47–79 Pa, respectively. The general trend showed a slight increase in G' across the frequency spectrum, indicating frequency-dependent viscoelasticity [60, 61]. This behavior is likely due to

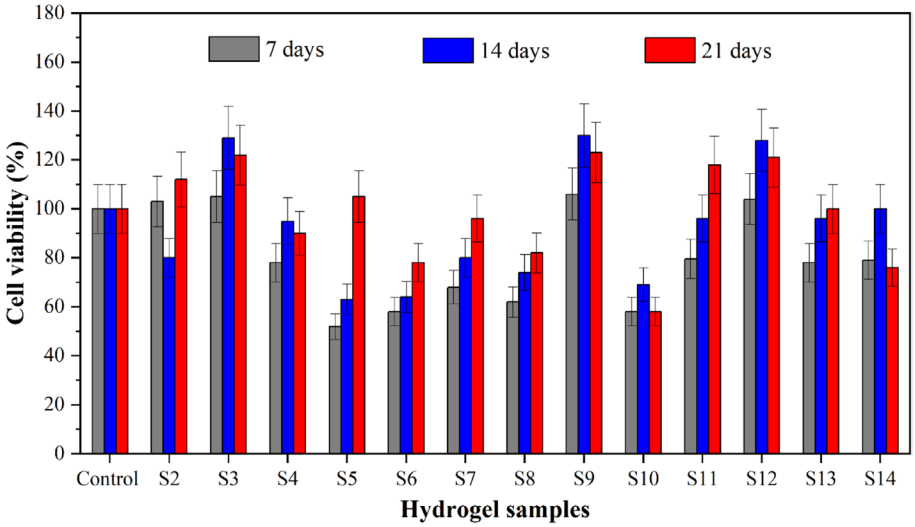

FIGURE 8 | MTS viability assay on Gingival Mesenchymal stem cells at 37°C during 7, 14, and 21 days in the presence of CS/PT/D-BC injectable hydrogels. [Color figure can be viewed at wileyonlinelibrary.com]

the time-dependent regeneration of kinetically unstable crosslinks. Remarkably, the variations in G' and G'' across S1–S15 correlate with changes in the degree of crosslinking, which influences macromolecular chain mobility [62]. The proximity of G' and G'') values further reflects the shear-thinning nature of the hydrogels. Among the tested samples, S3, S9, and S12 exhibited the highest G' and G'' values for varying concentrations of CS, PT, and D-BC, respectively.

3.8 | Biocompatibility and Antibacterial Activity of CS/PT/D-BC IHs

3.8.1 | Biocompatibility

To evaluate the potential of the CS/PT/D-BC injectable hydrogel system for sustained drug delivery and as a scaffold supporting cell growth, the viability and proliferation of GMS cells were assessed using the MTS metabolic assay in vitro. GMS cells were cultured with various hydrogel compositions for 21 days, and viability was measured at 7-day intervals. Results are presented in Figure 8a. Cells cultured without hydrogels served as the control group for normalization. As shown in Figure 8, samples S2, S3, S4, S9, S11, S12, S13, and S15 supported cell proliferation over the 21-day period, with viability exceeding 70%, while other samples exhibited reduced viability, suggesting potential cytotoxicity. Particularly, GMS cells seeded on S3, S9, and S12 maintained > 100% viability throughout, indicating strong biocompatibility. Sample S3, composed of 1% (w/w) CS, 1.5% (w/w) PT, and 0.5% (w/w) D-BC, was identified as the optimal formulation. Samples with higher CS or PT content (e.g., S5 and S10) showed reduced viability, implying potential cytotoxic thresholds. While samples S13–S15 with higher D-BC contents still showed high viability, slightly reduced performance compared to S3 may be due to increased stiffness, which can impair cell adhesion and spreading. Conversely, S11, with lower D-BC content than S3, exhibited marginally reduced viability, likely due to diminished structural support for cells. Overall, the results suggest that hydrogel formulation S3 offers the most favorable environment for GMS cell viability and proliferation, making it the most promising scaffold candidate for biomedical applications.

3.8.2 | Antibacterial Activity

To assess the antibacterial performance of the developed CS/PT/D-BC injectable hydrogel systems, hydrogel samples with varying concentrations of chitosan (S1–S5) were tested against both Gram-positive (*Staphylococcus aureus*) and Gram-negative (*Escherichia coli*) bacteria. Chitosan is known for its intrinsic antimicrobial properties, making it a promising candidate for biomedical applications. As shown in Figure 9, all tested samples demonstrated visible zones of inhibition against *S. aureus*, with increasing chitosan content (0.25%–2.0% w/w) resulting in more pronounced antibacterial effects. In contrast, minimal or no inhibition was observed against *E. coli*, with the exception of sample S5, which exhibited a weak inhibition zone measuring 0.50 ± 0.10 mm.

This differential activity can be attributed to both the physicochemical properties of the hydrogel system and the structural differences between Gram-positive and Gram-negative bacteria. Chitosan's antimicrobial mechanism primarily involves electrostatic interactions between its protonated amino groups (NH_3^+) and the negatively charged components of bacterial cell membranes. These interactions disrupt membrane integrity, leading to increased permeability, leakage of intracellular components, and ultimately cell death [48]. In Gram-positive bacteria, such as *S. aureus*, the thick peptidoglycan layer enriched with negatively charged teichoic acids facilitates stronger interactions with chitosan, enhancing antibacterial efficacy. Conversely, Gram-negative bacteria like *E. coli* possess an additional outer membrane composed of lipopolysaccharides that act as a barrier, limiting the interaction between chitosan and the cell envelope, and thereby reducing its antibacterial activity [63, 64]. The use of high molecular weight chitosan in this study further contributes to its antimicrobial effect, as it enables a greater interaction surface and a stronger

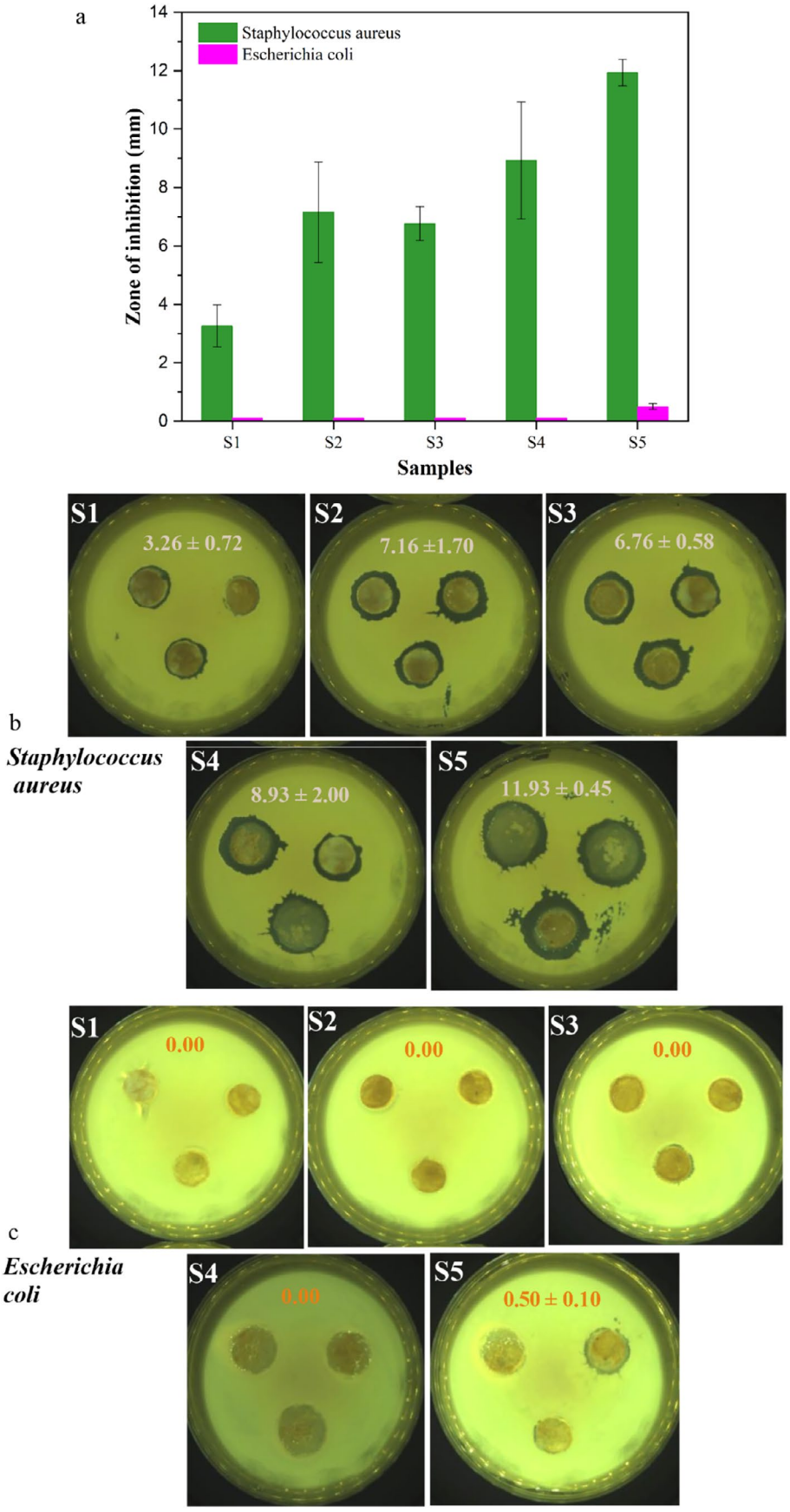

FIGURE 9 | (a) Zone of inhibition for the different injectable hydrogels (S1–S5) for varying concentrations of chitosan (0.25%–2.0% w/w). Visual image of antibacterial activity in the presence of (b) *Staphylococcus aureus* (Gram positive) and (c) *Escherichia coli* (Gram negative) *bacteria*. (Value inserts on the images represent the zone of inhibition in mm). [Color figure can be viewed at wileyonlinelibrary.com]

binding affinity with microbial membranes. The observed antibacterial activity, particularly against Gram-positive bacteria, highlights the potential of CS/PT/D-BC hydrogels in clinical applications where localized infection control is critical, such as in wound dressings, oral and maxillofacial scaffolds, or post-surgical implants. Overall, the results suggest that tailoring chitosan concentration within the hydrogel matrix not only modulates mechanical and biological properties but also enables the development of multifunctional biomaterials with inherent antibacterial capacity. Further optimization, including the incorporation of synergistic antimicrobial agents or surface modifications, could broaden the spectrum of activity and enhance usability in diverse biomedical settings.

3.9 | Research Perspectives in Terms of Social/Health Care Aspects

The development of dynamic IHs for treating soft tissue conditions has garnered considerable interest in biomaterials research. From both social and healthcare perspectives, polysaccharide-based IHs present promising yet complex opportunities. With increasing global emphasis on sustainable healthcare solutions and resource-efficient materials, IHs offer a unique advantage due to their minimally invasive application, ease of use, and potential for targeted therapy. In this context, the CS/PT/D-BC IH system exemplifies a cost-effective and socially beneficial biomedical material. These hydrogels are formulated entirely from bio-based, plant-derived components—chitosan, pectin, and bacterial cellulose—without the use of toxic crosslinking agents. The preparation process is simple, stable, and yields biocompatible materials suitable for clinical use.

Key benefits of the CS/PT/D-BC IH system include:

- Bio-based formulation, which is prepared without synthetic crosslinkers or harmful additives.
- Biocompatibility that depicts safety for integration with human tissue.
- Cost-efficiency that describes affordability and readily available raw materials.
- Eco-friendliness shows the non-toxic and sustainable sources that reduce environmental impact.
- Scalable production based on straightforward synthesis supports wider accessibility.

These attributes make the CS/PT/D-BC IH system well-suited for a range of soft tissue applications, including drug delivery, wound dressing, periodontal regeneration, and bone repair, while minimizing patient risk and healthcare costs. The broader adoption of such hydrogels could contribute significantly to global health equity, particularly in low-resource settings [65–67]. To advance this technology from laboratory research to clinical practice, future efforts should focus on regulatory pathways, translational studies, and interdisciplinary collaboration. Doing so will not only validate their therapeutic efficacy but also maximize their societal and economic impact.

4 | Conclusions

This study presents the development and preliminary evaluation of a self-crosslinkable, injectable hydrogel system based on CS, PT, and D-BC, designed to support soft tissue regeneration. The hydrogels were synthesized via a straightforward and reproducible method that leveraged both physical and chemical interactions, with D-BC serving as a natural crosslinker. This approach eliminated the need for synthetic agents and contributed to the system's biocompatibility. The CS/PT/D-BC injectable hydrogels exhibited favorable physicochemical and biological properties, including shear-thinning behavior, strong gel stability, thermal resilience, and high water retention. Structural features such as tunable porosity and swelling capacity, adjustable through polymer ratios, supported effective cellular proliferation. The hydrogels remained stable under physiological conditions, demonstrated antibacterial activity (especially against *Staphylococcus aureus*), and achieved over 80% cell viability in MTS assays, confirming their suitability for use as injectable scaffolds in soft tissue repair, particularly within oral and maxillofacial applications.

To further advance this system toward clinical relevance, ongoing research will address key limitations. These include optimizing the multi-polymer composition to enhance mechanical strength and biological responsiveness, as well as expanding cytocompatibility studies to include human dermal fibroblasts (HDFs) and pre-osteoblast MC3T3-E1 cells. Additionally, broader-spectrum antimicrobial evaluations, including Gram-negative bacteria and fungi, will be pursued. These efforts aim to build a more comprehensive understanding of the hydrogel's performance and reinforce its applicability in diverse tissue engineering and regenerative medicine settings.

Author Contributions

Nabanita Saha: conceptualization (supporting), methodology (supporting), project administration (supporting), validation (supporting), writing – original draft (supporting), writing – review and editing (supporting). **Fahanwi Asabuwa Ngwabebhoh:** conceptualization (supporting), data curation (supporting), formal analysis (supporting), investigation (supporting), methodology (supporting), writing – original draft (supporting), writing – review and editing (supporting). **Oyunchimeg Zandraa:** conceptualization (supporting), data curation (supporting), formal analysis (supporting), methodology (supporting), writing – original draft (supporting). **Mainak Chaudhuri:** data curation (supporting), formal analysis (supporting), methodology (supporting), writing – original draft (supporting). **Nibedita Saha:** data curation (supporting), formal analysis (supporting), writing – original draft (supporting). **Diana Solovyov:** data curation (supporting), formal analysis (supporting), validation (supporting). **Girts Salms:** data curation (supporting), formal analysis (supporting), project administration (supporting), validation (supporting). **Arita Dubnika:** funding acquisition (supporting), project administration (supporting), validation (supporting), writing – review and editing (supporting). **Alejandro Sosnik:** funding acquisition (supporting), project administration (supporting), validation (supporting), writing – review and editing (supporting). **Tomas Saha:** funding acquisition (supporting), project administration (supporting), validation (supporting), writing – review and editing (supporting). **Petr Saha:** funding acquisition (supporting), project administration (supporting), validation (supporting), writing – review and editing (supporting).

Acknowledgments

The TBU authors acknowledge the financial support received from Ministry of Education, Youth and Sports of the Czech Republic—DKRVO (RP/CPS/2024-28/005) and Technology Agency of the Czech Republic (TACR)—M-ERA.NET (TH71020005) project entitled "*Bioactive injectable hydrogels for soft tissue regeneration after reconstructive maxillofacial surgeries* (INJECT-BIO)". The associated Israel partner of the project is also acknowledging the support of the Ministry of Science and Technology of Israel (grant #317330-3), and the Latvian partner acknowledges the funding from the Latvian Council of Science agreement No. ES RTD/2020/14 and Horizon 2020 under grant No. 857287. Doctoral student Mainak Chaudhuri acknowledges the financial support of the IGA project (IGA/CPS/2022/002). Alejandro Sosnik thanks the support of the Tamara and Harry Handelsman Academic Chair. Open access publishing facilitated by Univerzita Tomase Bati ve Zline, as part of the Wiley - CzechELib agreement.

Ethics Statement

The study on isolated gingival mesenchymal stem cells (GMSCs) was conducted according to the guidelines of the Declaration of Helsinki and approved by the Research Ethics Committee at Riga Stradins University, Latvia, Permission Nr.6-1/12/47, 26.11.2020, and was in accordance with the principle of informed consent. The privacy rights of human subjects are always observed carefully.

Conflicts of Interest

The authors declare no conflicts of interest.

Data Availability Statement

All data will be made available upon reasonable request.

References

1. T.-H. Huang, J.-Y. Chen, W.-H. Suo, et al., "Unlocking the Future of Periodontal Regeneration: An Interdisciplinary Approach to Tissue Engineering and Advanced Therapeutics," *Biomedicine* 12 (2024): 1090.

2. A. V. Singh, V. Chandrasekar, V. M. Prabhu, et al., "Sustainable Bioinspired Materials for Regenerative Medicine: Balancing Toxicology, Environmental Impact, and Ethical Considerations," *Biomedical Materials* 19 (2024): 060501.

3. P. Shakoori, Q. Zhang, and A. D. Le, "Applications of Mesenchymal Stem Cells in Oral and Craniofacial Regeneration," *Oral and Maxillofacial Surgery Clinics of North America* 29 (2017): 19.

4. N. Muzzio, S. Moya, and G. J. P. Romero, "Multifunctional Scaffolds and Synergistic Strategies in Tissue Engineering and Regenerative Medicine," *Pharmaceutics* 13 (2021): 13, 792.

5. Z. Sheikh, N. Hamdan, Y. Ikeda, M. Grynpas, B. Ganss, and M. Glogauer, "Natural Graft Tissues and Synthetic Biomaterials for Periodontal and Alveolar Bone Reconstructive Applications: A Review," *Biomaterals Research* 21 (2017): 9.

6. O. S. Janjua, S. M. Qureshi, M. S. Shaikh, et al., "Autogenous Tooth Bone Grafts for Repair and Regeneration of Maxillofacial Defects: A Narrative Review," *International Journal of Environmental Research and Public Health* 19 (2022): 3690.

7. G. Morello, G. De Iaco, G. Gigli, A. Polini, and F. Gervaso, "Chitosan and Pectin Hydrogels for Tissue Engineering and in Vitro Modeling," *Gels* 9 (2023): 132.

8. J. C. Melville, B. Rethman, R. Rattan, et al., "Innovations in Maxillofacial Reconstruction and Tissue Engineering," in *Oral and Maxillofacial Surgery* ed. L. Andersson, D. G. Krishnan and Z. S. Peacock (Wiley, 2025), 711.

9. Y. Gu, Y. Yang, J. Yuan, et al., "Polysaccharide-Based Injectable Hydrogels With Fast Gelation and Self-Strengthening Mechanical Kinetics for Oral Tissue Regeneration," *Biomacromolecules* 24 (2023): 3345–3356.

10. C. Qian, T. Zhang, J. Gravesande, C. Baysah, X. Song, and J. Xing, "Injectable and Self-Healing Polysaccharide-Based Hydrogel for pH-Responsive Drug Release," *International Journal of Biological Macromolecules* 123 (2019): 140–148.

11. H. F. Darge, A. T. Andrgie, H.-C. Tsai, and J.-Y. Lai, "Polysaccharide and Polypeptide Based Injectable Thermo-Sensitive Hydrogels for Local Biomedical Applications," *International Journal of Biological Macromolecules* 133 (2019): 545–563.

12. N. Parvin, S. W. Joo, and T. K. Mandal, "Injectable Biopolymer-Based Hydrogels: A Next-Generation Platform for Minimally Invasive Therapeutics," *Gels* 11 (2025): 383.

13. A. R. Pereira, P. C. Pires, H. Hameed, et al.,"Injectable Nanocomposite Hydrogels for Targeted Intervention in Cancer, Wound Healing, and Bone and Myocardial Tissue Engineering," *Drug Delivery and Translational Research* (2025): 1–84.

14. A. Sosnik and K. P. Seremeta, "Polymeric Hydrogels as Technology Platform for Drug Delivery Applications," *Gels* 3 (2017): 25.

15. E. J. Delgado-Pujol, G. Martínez, D. Casado-Jurado, et al., "Hydrogels and Nanogels: Pioneering the Future of Advanced Drug Delivery Systems," *Pharmaceutics* 17 (2025): 215.

16. D.-q. Li, M. Tohti, Y.-s. Fu, et al., "Aldehyde Group Pendant-Grafted Pectin-Based Injectable Hydrogel," *International Journal of Biological Macromolecules* 264 (2024): 130453.

17. B.-D. Zheng, J. Ye, Y.-C. Yang, Y.-Y. Huang, and M.-T. Xiao, "Self-Healing Polysaccharide-Based Injectable Hydrogels With Antibacterial Activity for Wound Healing," *Carbohydrate Polymers* 275 (2022): 118770.

18. J. H. Lee, "Injectable Hydrogels Delivering Therapeutic Agents for Disease Treatment and Tissue Engineering," *Biomaterials Research* 22 (2018): 27.

19. Y. Chao, Q. Chen, and Z. Liu, "Smart Injectable Hydrogels for Cancer Immunotherapy," *Advanced Functional Materials* 30 (2020): 1902785.

20. S. Wang, H. Zheng, L. Zhou, et al., "Nanoenzyme-Reinforced Injectable Hydrogel for Healing Diabetic Wounds Infected With Multidrug Resistant Bacteria," *Nano Letters* 20 (2020): 5149–5158.

21. S. Liu, R. Guo, C. Li, et al., "POSS Hybrid Hydrogels: A Brief Review of Synthesis, Properties and Applications," *European Polymer Journal* 143 (2021): 110180.

22. S. Shekhar, V. Chaudhary, B. Sharma, A. Kumar, A. K. Bhagi, and K. P. Singh, "Sustainable Polysaccharide Hydrogels Based on Dynamic Schiff Base Linkages as Versatile Building Blocks for Fabricating Advanced Functional Materials," *Journal of Polymers and the Environment* 31 (2023): 1257–1278.

23. D. Nanda, D. Behera, S. S. Pattnaik, and A. K. Behera, "Advances in Natural Polymer-Based Hydrogels: Synthesis, Applications, and Future Directions in Biomedical and Environmental Fields," *Discover Polymers* 2 (2025): 6.

24. I. N. Weerarathna, P. Kumar, A. Luharia, and G. Mishra, "Engineering With Biomedical Sciences Changing the Horizon of Healthcare—A Review," *Bioengineered* 15 (2024): 2401269.

25. N. Chen, H. Wang, C. Ling, W. Vermerris, B. Wang, and Z. Tong, "Cellulose-Based Injectable Hydrogel Composite for pH-Responsive and Controllable Drug Delivery," *Carbohydrate Polymers* 225 (2019): 115207.

26. O. Amponsah, P. S. A. Nopuo, F. A. Manga, N. B. Catli, and K. Labus, "Future-Oriented Biomaterials Based on Natural Polymer Resources: Characteristics, Application Innovations, and Development Trends," *International Journal of Molecular Sciences* 26 (2025): 5518.

27. K. Y. Wu, J. K. Fujioka, P. Daigle, and S. D. Tran, "The Use of Functional Biomaterials in Aesthetic and Functional Restoration in Orbital Surgery," *Journal of Functional Biomaterials* 15 (2024): 33.

28. X. Du, Y. Liu, X. Wang, et al., "Injectable Hydrogel Composed of Hydrophobically Modified Chitosan/Oxidized-Dextran for Wound Healing," *Materials Science and Engineering: C* 104 (2019): 109930.

29. S. Almawash, S. K. Osman, G. Mustafa, and M. A. El Hamd, "Current and Future Prospective of Injectable Hydrogels—Design Challenges and Limitations," *Pharmaceuticals* 15 (2022): 371.

30. H. Zhao, Y. Zhang, C. Zhou, C. Zhang, and B. Liu, "Engineering pH Responsive Carboxyethyl Chitosan and Oxidized Pectin -Based Hydrogels With Self-Healing, Biodegradable and Antibacterial Properties for Wound Healing," *International Journal of Biological Macromolecules* 253 (2023): 127364.

31. M. T. P. Paiva, J. O. F. Kishima, J. B. M. D. Silva, J. Mantovan, F. G. Colodi, and S. Mali, "Crosslinking Methods in Polysaccharide-Based Hydrogels for Drug Delivery Systems," *Biomedical Materials & Devices* 2 (2024): 288–306.

32. V. G. Muir and J. A. Burdick, "Chemically Modified Biopolymers for the Formation of Biomedical Hydrogels," *Chemical Reviews* 121 (2020): 10908.

33. K. A. Kristiansen, A. Potthast, and B. E. Christensen, "Periodate Oxidation of Polysaccharides for Modification of Chemical and Physical Properties," *Carbohydrate Research* 345 (2010): 1264–1271.

34. F. A. Ngwabebhoh, O. Zandraa, R. Patwa, N. Saha, Z. Capáková, and P. Saha, "Self-Crosslinked Chitosan/Dialdehyde Xanthan Gum Blended Hypromellose Hydrogel for the Controlled Delivery of Ampicillin, Minocycline and Rifampicin," *International Journal of Biological Macromolecules* 167 (2021): 1468–1478.

35. E. S. Madivoli, P. G. Kareru, A. N. Gachanja, S. M. Mugo, and D. S. Makhanu, "Synthesis and Characterization of Dialdehyde Cellulose Nanofibers From O. Sativa Husks," *SN Applied Sciences* 1 (2019): 723.

36. D. Paiva, C. Gonçalves, I. Vale, M. M. S. M. Bastos, and F. D. Magalhães, "Oxidized Xanthan Gum and Chitosan as Natural Adhesives for Cork," *Polymers* 8 (2016): 8, 259.

37. G. Kowalski, K. Kijowska, M. Witczak, Ł. Kuterasiński, and M. Łukasiewicz, "Synthesis and Effect of Structure on Swelling Properties of Hydrogels Based on High Methylated Pectin and Acrylic Polymers," *Polymers* 11 (2019): 114.

38. P. Kotcharat, P. Chuysinuan, T. Thanyacharoen, S. Techasakul, and S. Ummartyotin, "Development of Bacterial Cellulose and Polycaprolactone (PCL) Based Composite for Medical Material," *Sustainable Chemistry and Pharmacy* 20 (2021): 100404.

39. R. S. Wong, M. Ashton, and K. Dodou, "Effect of Crosslinking Agent Concentration on the Properties of Unmedicated Hydrogels," *Pharmaceutics* 7 (2015): 305–319.

40. D. R. C. Fabian, S. Durpekova, M. Dusankova, et al., "Renewable Whey-Based Hydrogel With Polysaccharides and Polyvinyl Alcohol as a Soil Amendment for Sustainable Agricultural Application," *International Journal of Biological Macromolecules* 259 (2024): 129056.

41. W. Chen, S. Yuan, J. Shen, Y. Chen, and Y. Xiao, "A Composite Hydrogel Based on Pectin/Cellulose via Chemical Cross-Linking for Hemorrhage," *Frontiers in Bioengineering and Biotechnology* 8 (2021): 627351.

42. H. T. Nguyen, F. A. Ngwabebhoh, N. Saha, T. Saha, and P. Saha, "Gellan Gum/Bacterial Cellulose Hydrogel Crosslinked With Citric Acid as an Eco-Friendly Green Adsorbent for Safranin and Crystal Violet Dye Removal," *International Journal of Biological Macromolecules* 222 (2022): 77–89.

43. M. Muchová, L. Münster, Z. Capáková, V. Mikulcová, I. Kuřitka, and J. Vícha, "Design of Dialdehyde Cellulose Crosslinked Poly(Vinyl Alcohol) Hydrogels for Transdermal Drug Delivery and Wound Dressings," *Materials Science and Engineering: C* 116 (2020): 111242.

44. S. Khan and N. M. Ranjha, "Effect of Degree of Cross-Linking on Swelling and on Drug Release of Low Viscous Chitosan/Poly(Vinyl Alcohol) Hydrogels," *Polymer Bulletin* 71 (2014): 2133–2158.

45. L. Deng, B. Wang, W. Li, Z. Han, S. Chen, and H. Wang, "Bacterial Cellulose Reinforced Chitosan-Based Hydrogel With Highly Efficient Self-Healing and Enhanced Antibacterial Activity for Wound Healing," *International Journal of Biological Macromolecules* 217 (2022): 77–87.

46. G.-W. Oh, I.-W. Choi, W. S. Park, et al., "Preparation and Properties of Physically Cross-linkedPVA/Pectin Hydrogels Blended at Different Ratios for Wound Dressings," *Journal of Applied Polymer Science* 139 (2022): 51696.

47. Q. F. Dang, J. Q. Yan, J. J. Li, X. J. Cheng, C. S. Liu, and X. G. Chen, "Controlled Gelation Temperature, Pore Diameter and Degradation of a Highly Porous Chitosan-Based Hydrogel," *Carbohydrate Polymers* 83 (2011): 171–178.

48. S. Khattak, X.-T. Qin, L.-H. Huang, Y.-Y. Xie, S.-R. Jia, and C. Zhong, "Preparation and Characterization of Antibacterial Bacterial Cellulose/Chitosan Hydrogels Impregnated With Silver Sulfadiazine," *International Journal of Biological Macromolecules* 189 (2021): 483–493.

49. A. Çay, M. Miraftab, and E. Perrin Akçakoca Kumbasar, "Characterization and Swelling Performance of Physically Stabilized Electrospun Poly(Vinyl Alcohol)/chitosan Nanofibres," *European Polymer Journal* 61 (2014): 253–262.

50. G. Patroklou, E. Triantafyllopoulou, P.-E. Goula, et al., "pH-Responsive Hydrogels: Recent Advances in Pharmaceutical Applications," *Polymers* 17 (2025): 1451.

51. M. H. Bhuiyan, A. N. Clarkson, and M. A. Ali, "Optimization of Thermoresponsive Chitosan/β-Glycerophosphate Hydrogels for Injectable Neural Tissue Engineering Application," *Colloids and Surfaces B: Biointerfaces* 224 (2023): 113193.

52. M. S. Dayal and J. M. Catchmark, "Mechanical and Structural Property Analysis of Bacterial Cellulose Composites," *Carbohydrate Polymers* 144 (2016): 447–453.

53. X. Zhao, P. Li, B. Guo, and P. X. Ma, "Antibacterial and Conductive Injectable Hydrogels Based on Quaternized Chitosan-Graft-Polyaniline/Oxidized Dextran for Tissue Engineering," *Acta Biomaterialia* 26 (2015): 236–248.

54. S. Tang, K. Chi, H. Xu, Q. Yong, J. Yang, and J. M. Catchmark, "A Covalently Cross-Linked Hyaluronic Acid/Bacterial Cellulose Composite Hydrogel for Potential Biological Applications," *Carbohydrate Polymers* 252 (2021): 117123.

55. L. Deng, K. Ou, J. Shen, et al., "Double Cross-Linked Chitosan/Bacterial Cellulose Dressing with Self-Healable Ability," *Gels* 9 (2023): 772.

56. X. Wang, R. Song, M. Johnson, et al., "An Injectable Chitosan-Based Self-Healable Hydrogel System as an Antibacterial Wound Dressing," *Materials* 14 (2021): 5956.

57. G. Stojkov, Z. Niyazov, F. Picchioni, and R. K. Bose, "Relationship between Structure and Rheology of Hydrogels for Various Applications," *Gels* 7 (2021): 255.

58. S. P. Chegini, J. Varshosaz, H. M. Sadeghi, A. Dehghani, and M. Minaiyan, "Shear Sensitive Injectable Hydrogels of Cross-Linked Tragacanthic Acid for Ocular Drug Delivery: Rheological and Biological Evaluation," *International Journal of Biological Macromolecules* 165 (2020): 2789–2804.

59. G. I. Kaya and F. Oytun, "Rheological Properties of İnjectable Hyaluronic Acid Hydrogels for Soft Tissue Engineering Applications," *Biointerface Research in Applied Chemistry* 11 (2020): 8424.

60. L. Chen, X. Deng, L. Tian, et al., "Preparation and Properties of Chitosan/Dialdehyde Sodium Alginate/Dopamine Magnetic Drug-Delivery Hydrogels," *Colloids and Surfaces A: Physicochemical and Engineering Aspects* 680 (2024): 132739.

61. T. Cui, Y. Sun, Y. Wu, et al., "Mechanical, Microstructural, and Rheological Characterization of Gelatin-Dialdehyde Starch Hydrogels Constructed by Dual Dynamic Crosslinking," *LWT - Food Science and Technology* 161 (2022): 113374.

62. T. Cui, Y. Wu, C. Ni, Y. Sun, and J. Cheng, "Rheology and Texture Analysis of Gelatin/Dialdehyde Starch Hydrogel Carriers for Curcumin Controlled Release," *Carbohydrate Polymers* 283 (2022): 119154.

63. N. Deng, Q. Li, and W. Wang, "Design and Fabrication of Nanocellulose-Chitosan Composite Hydrogels with Enhanced Mechanical and Antibacterial Properties," *Langmuir* 41 (2025): 13604.

64. F. Wahid, X.-H. Hu, L.-Q. Chu, S.-R. Jia, Y.-Y. Xie, and C. Zhong, "Development of Bacterial Cellulose/Chitosan Based Semi-Interpenetrating Hydrogels With Improved Mechanical and Antibacterial Properties," *International Journal of Biological Macromolecules* 122 (2019): 380–387.

65. Y. Li, H. Y. Yang, and D. S. Lee, "Biodegradable and Injectable Hydrogels in Biomedical Applications," *Biomacromolecules* 23 (2022): 609–618.

66. P. Bertsch, M. Diba, D. J. Mooney, and S. C. G. Leeuwenburgh, "Self-Healing Injectable Hydrogels for Tissue Regeneration," *Chemical Reviews* 123 (2023): 834–873.

67. B. Zhu, T. Zong, R. Zheng, et al., "Acid and Glutathione Dual-Responsive, Injectable and Self-Healing Hydrogels for Controlled Drug Delivery," *Biomacromolecules* 25 (2024): 1838.